

Intrusion of Kuroshio Water onto the Continental Shelf of the East China Sea

JOON-SOO LEE^{1*} and TAKESHI MATSUNO²

¹Department of Earth System Science and Technology, Kyushu University,
Kasuga-Koen, Kasuga 816-8580, Japan

²Research Institute for Applied Mechanics, Kyushu University,
Kasuga-Koen, Kasuga 816-8580, Japan

(Received 15 May 2006; in revised form 22 November 2006; accepted 22 November 2006)

As a fundamental study to evaluate the contribution of the Kuroshio to primary production in the East China Sea (ECS), we investigated the seasonal pattern of the intrusion from the Kuroshio onto the continental shelf of the ECS and the behavior of the intruded Kuroshio water, using the RIAM Ocean Model (RIAMOM). The total intruded volume transport across the 200m isobath line was evaluated as 2.74 Sv in winter and 2.47 Sv in summer, while the intruded transport below 80m was estimated to be 1.32 Sv in winter and 1.64 Sv in summer. Passive tracer experiments revealed that the main intrusion from the Kuroshio to the shelf area of the ECS, shallower than 80m, takes place through the lower layer northeast of Taiwan in summer, with a volume transport of 0.19 Sv. Comparative studies show several components affecting the intrusion of the Kuroshio across the 200 m isobath line. The Kuroshio water intruded less onto the shelf compared with a case without consideration of tide-induced bottom friction, especially northeast of Taiwan. The variations of the transport from the Taiwan Strait and the east of Taiwan have considerable effects on the intrusion of the Kuroshio onto the shelf.

Keywords:

- Intrusion of Kuroshio water,
- outflow from the Taiwan Strait,
- East China Sea,
- continental shelf.

1. Introduction

The East China Sea (ECS) is a marginal sea, surrounded by Korea, Japan, China, and Taiwan. The ECS has a vast continental shelf and is bordered by the Okinawa Trough with a maximum depth exceeding 2000 m (Fig. 1). The cold, fresh shelf water is distributed on the continental shelf, and the warm, saline Kuroshio water occupies the area around the shelf water.

Several researchers have studied the process of water and material exchange between the shelf and Kuroshio waters. Northeast of Taiwan, the Kuroshio Edge Exchange Processes (KEEP) project of Taiwan has contributed to our understanding of the Kuroshio intrusion and the current pattern. Liu *et al.* (1992) confirmed that the upwelling of the Kuroshio subsurface water near the northern tip of Taiwan is caused by the impingement of the Kuroshio

onto the continental shelf, and it is a year-round phenomenon. Chern and Wang (1992) suggested that the variation of the Kuroshio intrusion is closely correlated with the outflow from the Taiwan Strait. Based on the result of the Shipboard ADCP observation in summer, Tang *et al.* (1999) constructed a horizontal current pattern: a deflected Kuroshio mainstream to the east, an intrusion of Kuroshio water onto the continental shelf, and a counterclockwise circulation northeast of Taiwan. In addition, Tang *et al.* (2000) presented three complementary snapshots of the current patterns in summer and winter, and suggested that the flow pattern north of Taiwan is significantly affected by the seasonal migration of the Kuroshio. Due to the intrusion northeast of Taiwan, an abundance of nutrients can be released into the ECS. From calculations of the nutrient budget, Chen and Wang (1999) showed that the supply of nutrients from the Kuroshio is much greater than the river input.

At the location where the Kuroshio flows along the continental shelf break, it is known that the frontal eddy plays an important role in the intrusion from the Kuroshio. The detailed three-dimensional structure of the Kuroshio frontal eddy along the shelf edge of the ECS has been

* Corresponding author. E-mail: leejs@affrc.go.jp

Present address: Marine Productivity Division, National Research Institute of Fisheries Science, Fisheries Research Agency, Yokohama, Kanagawa 236-8648, Japan.

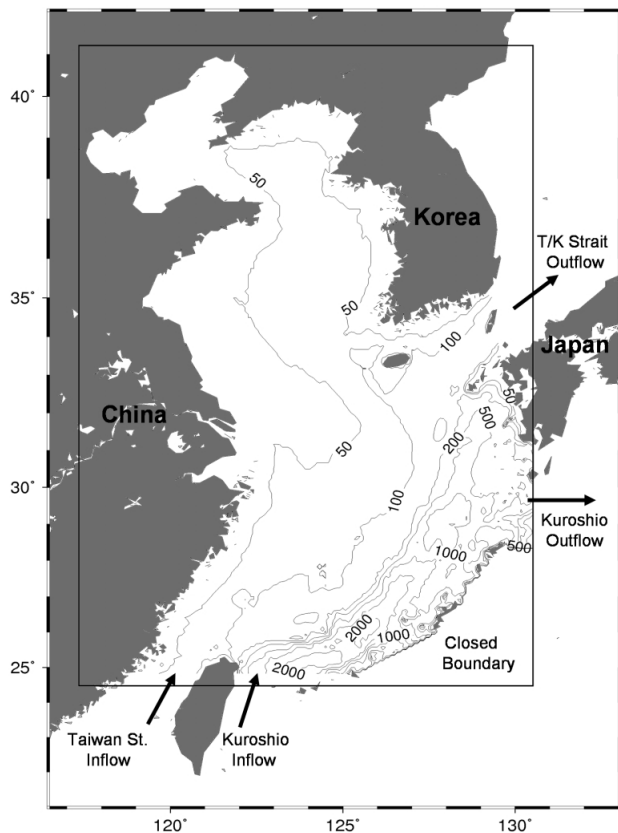


Fig. 1. Bathymetry of the Yellow and East China Seas and the model region.

revealed by Yanagi *et al.* (1998), who showed the nutrient transport across the shelf edge via the frontal eddy motion. On the other hand, Isobe *et al.* (2004) focused on the intrusion of shelf water into the Kuroshio subsurface layer due to the eddy motion.

Several studies using numerical models have also improved our understanding of the exchange process. Seung (1999) considered the dynamics of the shelfward intrusion of the oceanic upper water using a simple geostrophic adjustment model. He found that the sea level difference moves the front shelfward through a barotropic effect, while the density difference increases the width of the front through a baroclinic effect. Recently, using a triply nested ocean model with a maximum resolution of $1/18^\circ$, Guo *et al.* (2003) explained the seasonal change of the veering latitude of the Kuroshio southwest of Kyushu by the JEBAR (joint effect of baroclinicity and bottom relief) term of the vorticity equation, which is the interaction between the baroclinicity and bottom topography. With the same model, Guo *et al.* (2006) evaluated the temporal and spatial variations of the Kuroshio onshore flux across the shelf break of the ECS in terms of a depth-

averaged volume transport vector. They discussed the effect of the Ekman transport and the change in density field on the Kuroshio onshore flux. Isobe and Beardsley (2006) estimated the onshore cross-frontal transport at the shelf break of the ECS using the FVCOM (Finite Volume Coastal Ocean Model), which has finer resolution and resolves the complex bottom topography. They simulated frontal waves excited near the location where the bottom topography changes abruptly and also evaluated the onshore transport by passive tracer experiments, mainly focusing on the role of frontal waves.

The northern part of the ECS is a semi-closed area. If we assume that the fresh water flux through surface is 0, and the transport from rivers is negligible compared to the transport from the Taiwan Strait, net transport across the 200 m isobath line of the ECS is determined by the difference between the inflow transport through the Taiwan Strait and the outflow transport through the Tsushima/Korea Strait (T/K Strait).

In this study our major concern is shelfward net transport from the Kuroshio. Chen and Wang (1999) have already discussed the importance of the subsurface Kuroshio water as a nutrient source. The net transport along the 200 m isobath line, which was discussed by Guo *et al.* (2006), is significant for the volume transport budget itself. However, the shelfward net transport from the Kuroshio is important as a supply of nutrients for primary production from the viewpoint of the ecosystem.

In order to investigate the shelfward intruded Kuroshio water, we executed numerical model experiments for various cases and examined the intrusion process from the Kuroshio onto the continental shelf of the ECS. We revealed a seasonally varying spatial intrusion pattern of the Kuroshio across the 200 m isobath line of the ECS and calculated the net volume transport of the shelfward Kuroshio water using passive tracer experiments. In addition, we considered the Kuroshio branch current east of Taiwan, which was not included in the numerical experiment of Isobe and Beardsley (2006). Furthermore, the tide effect was also examined.

This numerical study could be used as a basic study of how much of the nutrients of the Kuroshio supplied into the shelf region of the ECS.

2. The Model

2.1 General description of the model

The RIAMOM (RIAM Ocean Model), which was developed in the Research Institute for Applied Mechanics in Kyushu University, is a 3-dimensional, primitive equation ocean model with a free surface. It employs a spherical coordinate horizontally with a staggered Arakawa B-grid and a z -coordinate vertically. In this model, the “slant advection” effect is considered in order

to represent the vertical advection effect of the horizontal momentum at the bottom topography as correctly as possible (Ishizaki and Motoi, 1999). As an advection scheme for tracers, the “modified split QUICK (MSQ) scheme (Webb *et al.*, 1998)” was adopted. In addition, the use of “partial step topography” facilitated a more realistic simulation near the bottom. The horizontal eddy viscosity and diffusivity were calculated using the Smagorinsky formula with a coefficient of 0.2. The vertical coefficients of eddy viscosity and diffusivity were calculated by solving the turbulent kinetic energy equation (Noh *et al.*, 2002).

The tide effect was parameterized by enhancing the background turbulence as vertical eddy diffusivity and viscosity and by increasing the bottom friction where the tidal current is strong. As the M2 tide is dominant over the ECS shelf, the amplitude of the M2 tidal current was used for the parameterization of the tide effect.

The increased vertical eddy diffusivity due to the M2 tide was calculated using the Munk-Anderson scheme, which depends on the Richardson number (Munk and Anderson, 1948):

$$K_z = K_o / (1 + \sigma Ri)^p \quad (1)$$

$$Ri = \frac{N^2}{(\partial U / \partial z)^2} \quad (2)$$

where σ and p are coefficients, assigned the value 3.33 and 1.5 respectively, K_o is the maximum diffusivity, $1.0 \times 10^{-3} \text{ m}^2\text{s}^{-1}$, and Ri is the Richardson number.

The vertical shear of the horizontal velocity in the Richardson number was replaced by James’ (1977, 1978) method (see also Lee *et al.*, 2006):

$$\left(\frac{\partial U}{\partial z}\right)^2 = \frac{1}{2} \left(\frac{A}{H-z}\right)^2 \quad (3)$$

where N is the Brunt-Väisälä frequency, H is the water depth, and $A = C_d^{1/2} V_t / k$. C_d is the bottom drag coefficient, 0.0025, k is the von Kármán constant, 0.41, and V_t is the amplitude of the M2 tidal current obtained from the NAO.99Jb model (Matsumoto *et al.*, 2000).

The vertical eddy viscosity due to the M2 tide was calculated by the James’ (1978) method, as follows:

$$A_z = A_o / \left(1 + \frac{p\sigma Ri}{p-1}\right)^{p-1} \quad (4)$$

where A_o is the maximum viscosity and it is assumed that $A_o = K_o$, following James (1978).

Table 1. Layer thickness and depth used in the model. Δz is layer thickness and z is depth.

Levels	Δz [m]	z [m]
1~6	5	30
7~13	10	100
14~23	20	300
24~33	40	700
34~38	80	1100
39	200	1300
40	200	1500
41	500	2000

The Richardson number is given by the same equation as (2). The enhanced vertical eddy diffusivity and viscosity due to the M2 tide were simply superposed on those calculated by the Noh scheme (Noh *et al.*, 2002).

Lee *et al.* (2000) showed the effectiveness of the linear bottom friction given by Hunter’s formula (1975) in the ECS. In order to consider the enhanced bottom friction due to the tidal stress, a linear-type bottom friction formulated by Hunter (1975) was adopted instead of a quadratic bottom friction:

$$\tau_{b\lambda} = \rho_o C_d \kappa u_b \quad (5)$$

$$\tau_{b\phi} = \rho_o C_d \kappa v_b \quad (6)$$

where $\tau_{b\lambda}$ and $\tau_{b\phi}$ are the zonal and meridional components of the bottom frictional stress, respectively. ρ_o is the sea water density, C_d is the bottom drag coefficient (0.0025), κ is the coefficient of the linear bottom friction, and u_b, v_b are the model velocity at the bottom in the zonal and meridional directions, respectively.

The linear bottom friction coefficient, κ , was given by time averaging the quadratic bottom friction term in the presence of strong tidal currents. In this study we applied a linear bottom friction coefficient used by Lee *et al.* (2000).

$$\kappa = 1.23 \sqrt{(\overline{u_t})^2 + (\overline{v_t})^2} \quad (7)$$

where $\overline{u_t}$ and $\overline{v_t}$ represent the depth-averaged M2 tidal velocity in the zonal and meridional directions, respectively. The zonal and meridional components of the M2 tidal current for the tide parameterization were obtained from the NAO.99Jb model (Matsumoto *et al.*, 2000).

2.2 Model domain and boundary conditions

The model region (Fig. 1) covers the entire Yellow and East China Seas. The horizontal resolution is $1/6^\circ$

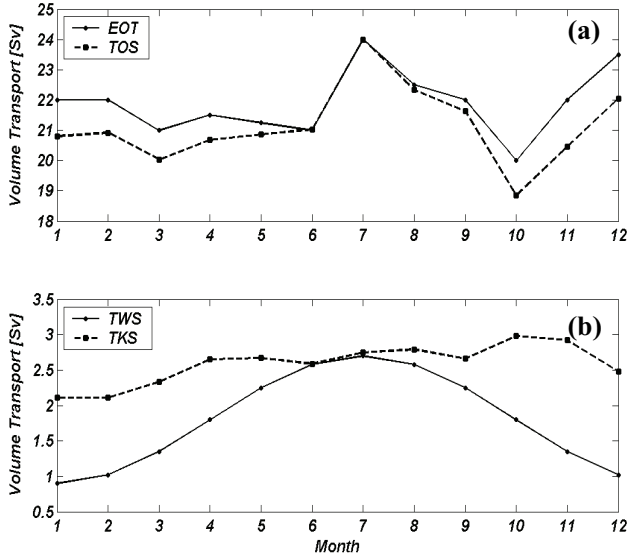


Fig. 2. Monthly value of the volume transports through (a) the east of Taiwan (EOT: solid line), the Tokara Strait (TOS: dashed line), (b) the Taiwan Strait (TWS: solid line), and the Tsushima/Korea Strait (TKS: dashed line).

and the number of vertical levels is 41 with a minimum depth of 10 m and a maximum depth of 2000 m (Table 1). We increased the vertical resolution near the sea surface. From the surface to a depth of 300 m, there are 23 vertical levels with 5 to 20 m spacing. The bottom topography is derived by the horizontal averaging of the Jtopo30 dataset from the Marine Information Research Center of the Japan Hydrographic Association (www.mirc.jha.or.jp/products/JTOPO30/). In spite of the high resolution, the Jtopo30 dataset only covers the eastern part of 120°E, so the Etopo5 dataset (NGDC, www.ngdc.noaa.gov/mgg/global/relief/ETOPO5/) is used for the remainder. The bottom topography of the model region is shown in Fig. 1. The Taiwan Strait, the east of Taiwan, the Tokara Strait, and the T/K Strait are the main open boundaries. The southeastern boundary along the Ryukyu Islands is closed.

Many scientists have suggested different volume transports through the Taiwan Strait, depending on the measuring time and position. The result of Wang *et al.* (2003) is used as an inflow volume transport of a control case for this study and the transport through the Taiwan Strait is set to 0.9 Sv in winter and 2.7 Sv in summer. Wang *et al.* (2003) estimated the volume transport from the empirical formula using the shipboard ADCP for 2.5 years and the along-strait wind data. Transports are interpolated as a sinusoidal curve. The seasonally varying transport east of Taiwan has a maximum of 24 Sv in summer with a weaker secondary maximum in winter, and a minimum of 20 Sv in fall (Lee *et al.*, 2001). They esti-

mated the volume transport from a sea level difference time series, a 7-year dataset from 1989 to 1996, between Ishigaki island in Japan and Keelung in Taiwan. The outflow transport of the T/K Strait varies monthly and is estimated from sea level differences, a 37-year dataset from 1965 to 2001, between Hakata and Busan (Takikawa and Yoon, 2005). The average volume transport through the eastern and western channels is 2.6 Sv.

The remnants of the inflow transport flow out through the Tokara Strait. Figure 2 shows the monthly variations of the volume transport through the Taiwan Strait, the east of Taiwan, and the T/K Strait. The density, derived from the temperature and salinity at each inflow boundary, determined the vertical geostrophic velocities using the thermal wind relation. The calculated geostrophic velocities are adjusted to meet the volume transports specified at the open boundaries. The inflow temperature and salinity were obtained from the climatology data of the World Ocean Atlas 2001 (WOA01) with a 1/4° grid resolution (Boyer *et al.*, 2002; Stephens *et al.*, 2002).

The heat flux at the sea surface was calculated using the Barnier method (Barnier *et al.*, 1995). The model heat flux appears as the sum of a climatological flux and a correction term proportional to the difference between the climatological sea surface temperature and the model surface temperature,

$$Q_{NET}(T_S) = Q_{NET}(T_S^{Clim}) + \left(\frac{\partial Q_{NET}}{\partial T} \right)_{T_S^{Clim}} (T_S^{Clim} - T_S) \quad (8)$$

where $Q_{NET}(T_S^{Clim})$ is the climatological flux, T_S^{Clim} is the climatological sea surface temperature, and T_S is the model surface temperature.

The heat flux was evaluated with a combination of the Southampton Oceanography Centre (SOC) climatological heat flux (Grist and Josey, 2003) and the sea surface temperature of the WOA01 climatology dataset with a relaxation time scale of ten days. The sea surface salinity was restored at the surface grid using the WOA01 climatology dataset. We adopted the monthly mean sea surface wind field which was computed from the weather charts for 1978–1995 (Na and Seo, 1998), and converted it into wind stress using the Large and Pond (1981) surface drag coefficient formulation.

The model was initialized from rest with zero sea level elevation and with an annual mean temperature and salinity taken from the WOA01 dataset. All forcing and boundary inputs were provided by monthly data and linearly interpolated to the model time step. After a spin up time of six years, passive tracers were released. An explanation of passive tracer experiments is given in Subsection 3.3.1.

In the Preliminary Experiment we discuss the tracer

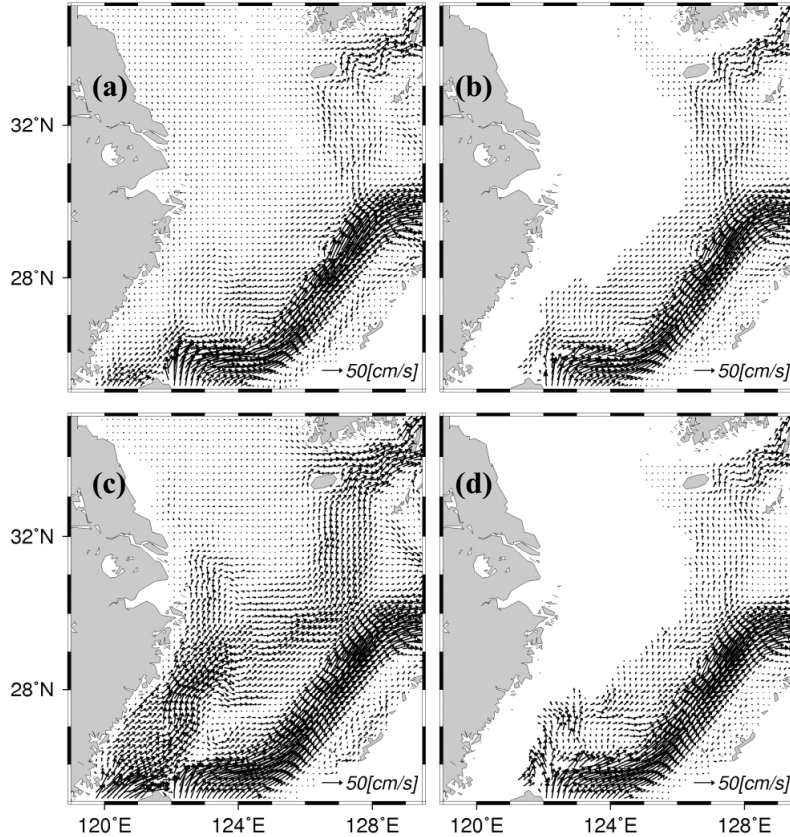


Fig. 3. Surface (2.5 m) and deeper layer (85 m) velocity fields of the seventh year of the control case (Case.1) in the ECS: (a) surface velocity field in winter, (b) deeper layer velocity field in winter, (c) surface velocity field in summer, (d) deeper layer velocity field in summer.

distribution released from the Taiwan Strait. The control case, Experiment 1, sets tracer release positions along the local sections of the 200 m isobath line and adopts the boundary conditions described in this section. Experiment 2 investigates the effects of tide, transport from the Taiwan Strait, and transport east of Taiwan, with detailed case studies. The cases are labeled Case.1 (control case) to Case.8.

3. Results

Hur *et al.* (1999) pointed out that the oceanographic season in the Yellow and East China Seas slightly lags the meteorological season. They defined four seasons based on the monthly T-S diagram: spring from April to June, summer from July to September, autumn from October to December, and winter from January to March. In this study we discuss the seasonal variation on the basis of this criterion, and the modeled winter and summer cases are represented by the results of February and August, respectively.

3.1 General features of the current field and comparison with the vertical section in the PN line

Researchers have suggested a schematic view of the current system based on observations using ADCPs, current meters, and satellite tracked drifters. Fang *et al.* (1991) analyzed historical current meter data above the continental shelf of the ECS and obtained similar northeastward current patterns for four seasons. More detailed current patterns of the ECS in summer were revealed by Katoh *et al.* (1996a, 1996b, 2000) using four round-trip ADCP surveys. Katoh *et al.* (1996a, b) presented detailed current structures west of Kyushu and the eastern continental shelf margin of the ECS, respectively. Moreover, Katoh *et al.* (2000) showed current distributions in the southern ECS where the outflow from the Taiwan Strait flows northeastward along the coast of China, and the Kuroshio branch current flows northward east of Taiwan with the anti-cyclonic eddy on its right. Lie *et al.* (1998) showed the separation of the Tsushima Warm Current from the Kuroshio using composite tra-

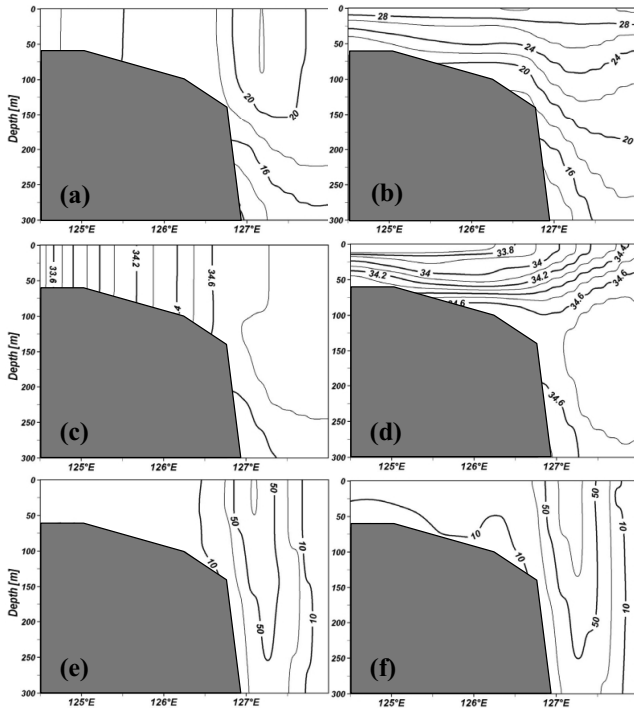


Fig. 4. Cross-sections of temperature [$^{\circ}\text{C}$], salinity, and along-shelf velocity [cm/s] along the PN-line for the modeled control case in winter and in summer: (a) temperature profile in winter, (b) temperature profile in summer, (c) salinity profile in winter, (d) salinity profile in summer, (e) along-shelf velocity in winter, (f) along-shelf velocity in summer. Thin solid line represents a middle value between two thick solid lines.

jectories of 172 drogued drifters.

The monthly averaged current distribution of the control case after a spin up is shown in Fig. 3. The model results of the seventh year successfully simulated the well-known currents such as the Kuroshio, the outflow from the Taiwan Strait, and the Kuroshio branch current.

The PN line in the ECS is a regular section observed by the Nagasaki Marine Observatory, and it provides a good measure for the model validation in the ECS. Figure 4 shows the modeled temperature, salinity, and along-shelf velocity fields in winter and in summer at the PN line. The temperature and salinity fields are similar to those of Oka and Kawabe (1998), seasonally averaged during 1988 to 1994, especially in summer, by displaying the same extent of intrusion range and thickness. The profiles of the along-shelf velocity component also provide a good picture of the structure of the Kuroshio in the ECS. Although the maximum velocity is smaller than the observed value, the velocity field around the Kuroshio and near the shelf-break matches well with those of Oka and Kawabe (1998).

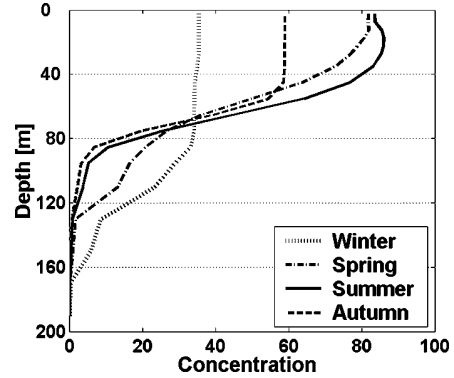


Fig. 5. Vertical profile of the average tracer concentration in the Preliminary Experiment. The tracer is horizontally averaged at the area where the water depth ranges from 100 m to 200 m along the shelf break west of 127°E .

Comparison of the model results with the PN line observations and the surface current distributions of Katoh *et al.* (1996a, 1996b, 2000) and Lie *et al.* (1998), confirms that the model well simulates the circulation in the ECS and the vertical density field around the shelf break. Based on the validation of the model, the results of the tracer experiments will be described.

3.2 Preliminary Experiment (Case.0—released from the Taiwan Strait)

In order to investigate the behavior of the outflow from the Taiwan Strait, the tracer was deployed for six years through the Taiwan Strait after a spin up time of six years. The concentration of the tracer was set to 100 and released into the model domain in which the concentration was entirely zero. The tracer concentration was governed by the same advection-diffusion equation that determined the temperature and salinity. No surface or bottom flux of the tracer was applied.

At the central part of the ECS, concentration of the tracer, which originated from the Taiwan Strait, reached a converged state having regular seasonal variation in the third year after deployment (not shown here). We analyzed the data of the sixth year after the release of the tracer and present the results as the preliminary study, as a similar experiment has already been carried out by Guo *et al.* (2006).

Figure 5 shows the vertical profile of the tracer concentration which is horizontally averaged at the area where the water depth ranges from 100 m to 200 m along the shelf break. The area was selected since it was expected to be a boundary between the outflow from the Taiwan Strait and the Kuroshio. The tracer from the Taiwan Strait is mainly distributed in the upper part of the shelf. The average tracer concentration falls to about 10

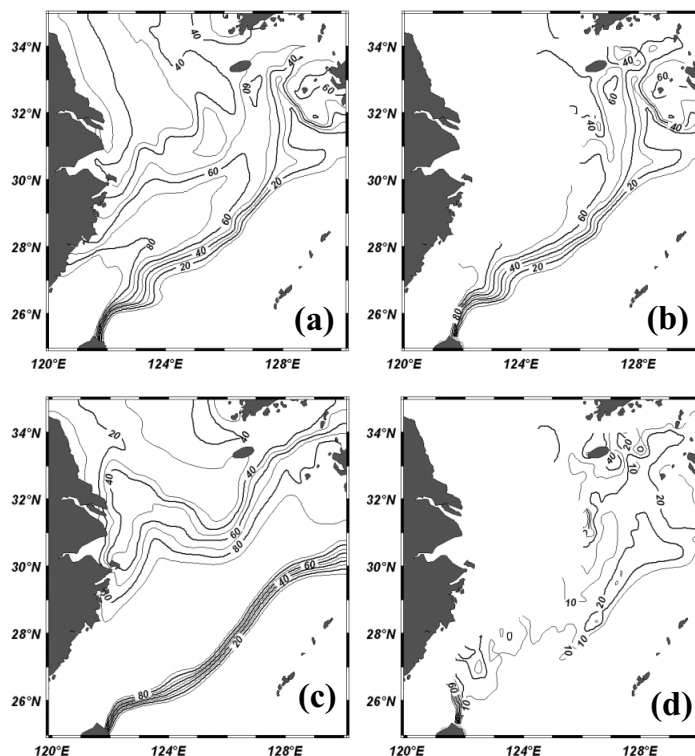


Fig. 6. Horizontal distributions of the tracers at the surface (2.5 m) and deeper layers (85 m) in the Preliminary Experiment: (a) winter distribution at the surface layer, (b) winter distribution at the deeper layer, (c) summer distribution at the surface layer, (d) summer distribution at the deeper layer.

percent in the summer at 80 m depth. Taking into account the fact that the depth of the Taiwan Strait is less than 60 m, the summer season with strong stratification by surface heating and relatively weak wind stress allows the water from the Taiwan Strait to be confined to just the upper layer. For simplicity, we divided the vertical section along the 200 m isobath line into an upper layer (0~80 m) and a lower one (80~200 m). We investigate the Kuroshio intrusion pattern based on this vertical partition.

The horizontal distributions of the tracers at depths of 2.5 m and 85 m are shown in Fig. 6. In winter, surface cooling and strong wind stress induce vigorous vertical mixing, making the water column homogeneous. The tracer from the Taiwan Strait is distributed in nearly the same area at the surface (2.5 m) and at a deeper layer (85 m). However, different patterns emerge in summer. With the increased inflow transport from the Taiwan Strait, the tracer from the Taiwan Strait covers the surface of the ECS widely. Unlike the surface, concentration of the tracer is remarkably reduced in the deeper layer (85 m). Because the model inflow boundaries are not only the Taiwan Strait but also east of Taiwan, the deeper layer would be filled with the tracer from east of Taiwan.

This experiment cannot give us clear information about the location of the vigorous intrusion, how much transport flows into the shelf area of the ECS from the Kuroshio, where the intruded Kuroshio water flows to, and so on. To answer these questions, we carried out Experiment 1.

3.3 Experiment 1 (Case.1—released from a 200 m-line: Control case)

3.3.1 Description of passive tracer experiments

In order to investigate the behavior of the Kuroshio water intruded onto the ECS shelf, we set the release position along the 200 m isobath line. The release position was divided into five local sections of 1 degree interval from 122°E to 127°E and one additional section from 127°E to 128.5°E. Moreover, each local section was divided into two vertical sections: upper layer (0~80 m) and lower layer (80~200 m).

The passive tracers were independent of each other but they moved in the same current field. A tracer which flowed down with the Kuroshio outside of the 200 m isobath line could intrude across other local sections along the 200 m line. To prevent this contamination by the same tracer from outside, when tracers were released along a

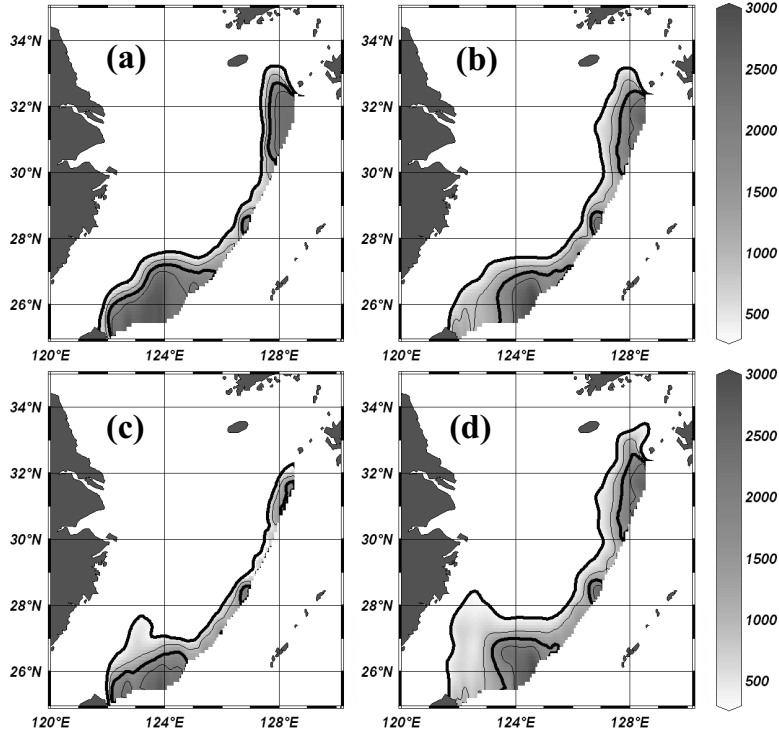


Fig. 7. Horizontal distributions of intruded tracer through the upper 80 m and below 80 m in winter and summer (Case.1): the tracers (a) released from 0~80 m in winter, (b) released from 80~200 m in winter, (c) released from 0~80 m in summer, (d) released from 80~200 m in summer. The unit of the vertically integrated tracer, [km^3], is omitted.

certain local section, the concentration of tracers along the other local section and from 128.5°E to Kyushu Island on the 200 m isobath line was fixed to 0. The tracers were deployed separately for 30 days through the local sections of the 200 m isobath line. The 30 day period was selected for the time that the tracers did not arrive at the T/K Strait. In this way, four seasonal cases were simulated. After a spin up time of six years, four sets of models were ready for the tracer experiments of the seventh year. With the additional calculations of 1 month for a winter case, 4 months for a spring case, 7 months for a summer case, and 10 months for an autumn, the tracers were released on the first day of February for the winter case, May for spring, August for summer, and November for autumn. To show the horizontal distribution of intruded water, we used a vertically integrated mass.

The vertically integrated mass is expressed as follows:

$$\int_V C \cdot dV \quad (9)$$

where C is the concentration of the tracer from 0 to 100, and V is the volume of each grid including the tracer. The unit is [km^3].

The intruded volume transport across the 200 m line could be calculated by the time derivative of the total amount of water including the passive tracer as demonstrated by Isobe and Beardsley (2006):

$$\frac{\partial}{\partial t} \left(\int_V \frac{C}{100} dV \right). \quad (10)$$

In the experiments where we investigate the behavior of the intruded tracer using the vertically integrated mass, we considered that the horizontal and vertical diffusions influenced the tracer, like temperature and salinity. However, if we calculate the volume transport using the tracer, the diffusions can lead to the wrong estimation of volume transport, especially regarding the tracer released from the local sections. So, for the calculation of the volume transport, we allowed the motion of tracer to be affected only by the advection, unlike Isobe and Beardsley (2006).

3.3.2 Behavior of the tracer intruded onto the ECS shelf

Figure 7 shows horizontal distributions of intruded tracer through the upper 80 m and below 80 m in winter and summer. The outer thick solid line represents the value of 300 [km^3], which is about 10% of maximum value.

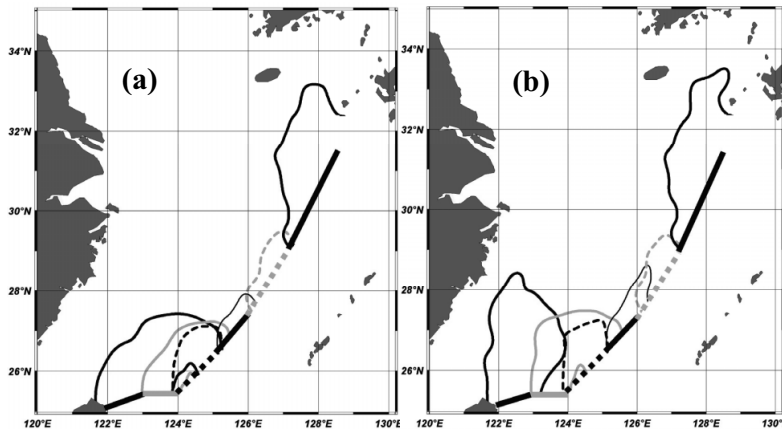


Fig. 8. Detailed spatial distribution of the intruded tracer through each local section after 30 days from the release at the 200 m isobath line: (a) in winter and (b) in summer. Thick solid or dashed lines with black or gray color along 200 m isobath line represent release positions. The color and shape of the contour lines are matched with the line representing the release positions along 200 m isobath line.

The unit of the vertically integrated tracer, [km^3], is omitted. The contour increments are 600. The value of 1500 is also represented by the thick solid line.

To specify the intrusion pattern of the control case, we investigate the detailed spatial distribution of the intruded tracer through each local section (Fig. 8). Each contour that is depicted by the different types of line represents the value of 300, as with the outer thick solid line of Fig. 7. Figure 8 clearly shows the region of the main intrusion as indicated by previous studies: northeast of Taiwan (e.g., Chen *et al.*, 1994; Tang *et al.*, 1999, 2000) and west of Kyushu (e.g., Lie and Cho, 1994; Hsueh *et al.*, 1996; Lie *et al.*, 1998). The intrusion from the Kuroshio in the central part of the 200 m line (124~127°E) is confined to the outer continental shelf. A large difference between winter and summer is seen in the distribution of the tracer intruded through 122~123°E. In winter, the tracer is limited south of 28°N, and extends eastward, while in the summer a part of the tracer intrudes northward into the shallow area. Where does the Kuroshio water intruded through 122~123°E flow to in winter and summer? There is a need to investigate the spatial variability of the intruded tracer with time. We executed an additional experiment at the end of a spin-up. The tracers were released for 90 days to show the behavior of each intruded tracer. To represent the behavior in each season, the tracers were released one month earlier than in Figs. 7 and 8: the first day of January for the winter case and that of July for summer.

Figure 9 shows the spatial distributions of the intruded tracer through the upper 80 m and below 80 m in winter and summer. The snapshot results of the tracer distribution were taken with a time interval of ten days. In winter, the pattern of the tracer extension is quite similar

in both cases (Figs. 9(a) and (b)). The tracer intruded northeast of Taiwan (122~123°E) and flows northeastward along the shelf edge. In summer, its distribution is quite different (Figs. 9(c) and (d)). First, the intruded tracer in the upper layer does not flow to the Tsushima/Korea Strait (Fig. 9(c)). The tracer cannot flow across the 29°N line. Unlike the upper layer, the tracer intruded through the lower layer below 80 m northeast of Taiwan (Fig. 9(d)). The tracers are divided into two major routes: along the shelf and along the small valley in the western ECS. A circle in the center indicates that the concentration of the tracer is relatively low because of the local topography bump. It takes about three months to reach the central part of ECS.

Kuroshio water which intruded through the lower layer of 122~123°E in the summer extended into the central part of the ECS. To examine other intrusions through different locations of the 200 m isobath line, we describe the tracer intruding through the lower layer of 123~124°E and 124~125°E in the summer. As shown in Fig. 10, the intruded Kuroshio water through the lower layer of 123~124°E flows down along the shelf edge, and the Kuroshio water through the lower layer of 124~125°E did not extend far, remaining mainly near the intrusion area of the shelf break. Although the intruded Kuroshio waters across the 200 m isobath line east of 125°E are not shown here, they too did not extend into the central part of ECS.

The observation results reported in Katoh *et al.* (2000) reveal the existence of a northward current northeast of Taiwan in summer. As shown in figure 3 of that paper, the high salinity water (>34.6 psu) detected by CTD observation can provide evidence that the intruded Kuroshio water is distributed below 70 m, even at the

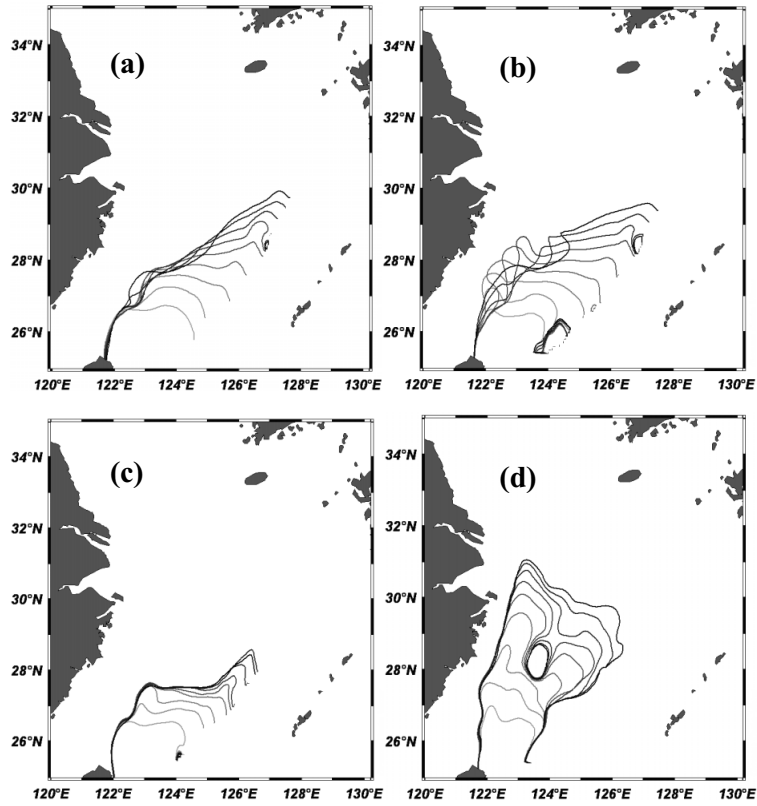


Fig. 9. Spatial variability of the intruded tracer through $122\sim 123^{\circ}\text{E}$ with a time interval of 10 days. The tone of line darkens with time: the tracers (a) released from $0\sim 80$ m in winter, (b) released from $80\sim 200$ m in winter, (c) released from $0\sim 80$ m in summer, (d) released from $80\sim 200$ m in summer.

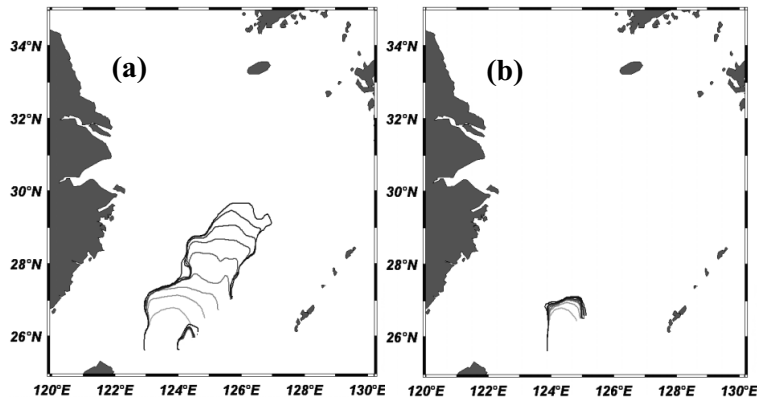


Fig. 10. Spatial variability of the intruded tracer (a) through $123\sim 124^{\circ}\text{E}$, (b) through $124\sim 125^{\circ}\text{E}$ at the 200 m isobath line with a time interval of 10 days. The tone of the line darkens with time.

mouth of the small valley on the western ECS, 28°N and 123°E . Although there is no current data near the small valley, the observed current data of the southern region, near 27°N and 123°E , show that a northward current of about $10\sim 20$ cm/s exists at a depth of 70 m, the upper

part of the high salinity water in figure 3 of Katoh *et al.* (2000). If there is a northward current of about $10\sim 20$ cm/s from the northeast of Taiwan, it takes $19\sim 38$ days from 25°N to 28°N as a straight line distance, which agrees well with the modeled time scale of one month

Table 2. Intruded total volume transport through 80~200 m and 0~200 m of the total and local sections for Case.1, including seasonal variations (Win = winter, Spr = spring, Sum = summer, Aut = autumn). S.A and A.A mean seasonal averaged and annual averaged volume transport, respectively. The volume transport unit is Sv (Sverdrup: 1 Sv = 10 m⁶/sec). “Ratio” denotes the ratio of the volume transport through 80~200 m to that through 0~200 m.

	122~123°E				123~127°E				127~128.5°E				Total			
	Win	Spr	Sum	Aut	Win	Spr	Sum	Aut	Win	Spr	Sum	Aut	Win	Spr	Sum	Aut
80~200 [m]																
S.A	0.41	0.38	0.45	0.32	0.42	0.67	0.72	0.74	0.49	0.46	0.47	0.48	1.32	1.51	1.64	1.54
A.A		0.39				0.64				0.48				1.5		
0~200 [m]																
S.A	1.34	0.94	1.05	1.05	0.54	0.82	0.88	1.08	0.86	0.67	0.54	0.71	2.74	2.43	2.47	2.84
A.A		1.1				0.83				0.7				2.62		
Ratio (%)																
S.A	30.6	40.4	42.9	30.5	77.8	81.7	81.8	68.5	57	68.7	87	67.6	48.2	62.1	66.4	54.2
A.A		36.1				77.5				70.1				57.7		

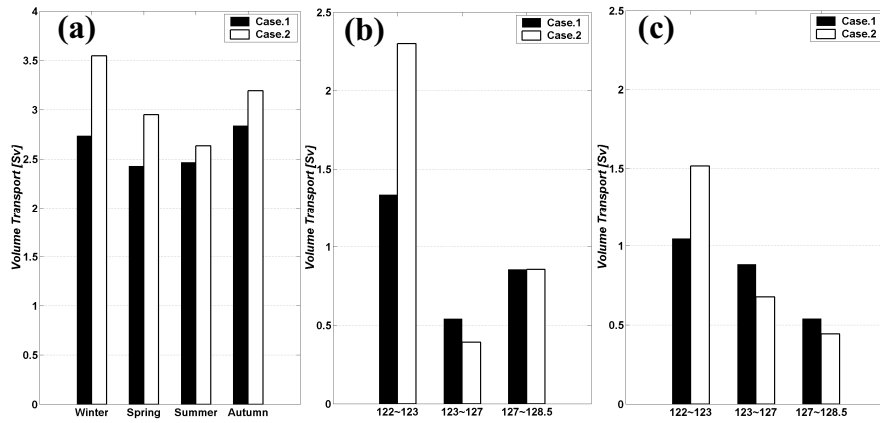


Fig. 11. Seasonal variation of the total intruded volume transport through the whole depth of the 200 m line (a), the transport through the local section in winter (b) and in summer (c) for Case.1 and Case.2.

depicted in Fig. 9(d). This suggests that the intruded Kuroshio water can exert a sufficient influence on the central ECS through the lower layer in summer.

3.3.3 Volume transport of the Kuroshio intrusion

In order to specify the Kuroshio intrusion, we calculated the quantitative value of the Kuroshio intrusion through the local sections. Table 2 shows the value of the intruded volume transport through 80~200 m and 0~200 m, including seasonal variations. The annual average of the Kuroshio intrusion is about 2.62 Sv and the intrusion increased in autumn and in winter, and decreased in spring and summer. However, the ratio of the transport through 80~200 m to that of 0~200 m was clearly increased in the summer (66.4%) compared with the winter value (48.2%).

In the previous section it was shown that the intrusion into the central part of ECS mainly occurs through the lower layer of 122~123°E in summer. The question

that arises is, “How much of the Kuroshio originated water flows into the central part of ECS?” To evaluate the volume transport in the central part of ECS, we define the central part of ECS as the “shelf area”. The shelf area in this paper is defined as the area shallower than 80 m south of 33°N, north of 28°N, and east of 122°E. After the previous tracer experiment for one month in summer, in which the tip of the intruded tracer reached the southern edge of the shelf area, the tracer is continuously released at the 200 m isobath line of 122~123°E for another month. The volume transport of Kuroshio water intruded into the shelf area is calculated by the tracer intruding into the shelf area for one month, using the same method as in the previous section. In this way, the volume transport of the intrusion into the shelf area is calculated for four seasons: 0 Sv for winter, 0.2 Sv for spring, 0.19 Sv for summer, and 0.08 Sv for autumn. This result indicates that

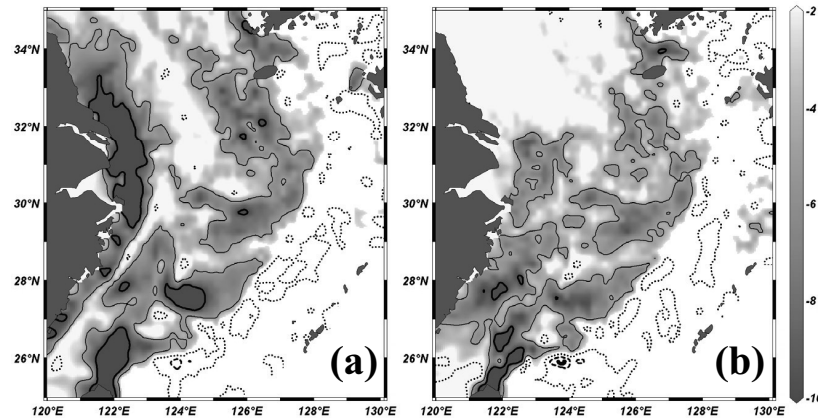


Fig. 12. Difference of velocity at the bottom layer (Case.1 minus Case.2): (a) in winter, (b) in summer. Unit is [cm/s] and minus value indicates bottom velocity at some point at which Case.1 is smaller than Case.2. Thick solid line represents a contour of -10 cm/s, thin solid line -5 cm/s, dotted line 0 cm/s, and thick dashed line 5 cm/s.

the intrusion of Kuroshio water into the shelf area starts in the spring and ends in autumn. The volume transport of the Kuroshio intrusion in summer, 0.19 Sv, is approximately three times the volume transport in summer from the Changjiang River, 0.06 Sv, signifying that the Kuroshio water intruded through the lower layer of $122\sim 123^\circ\text{E}$ can transport a great deal of nutrients to the shelf area, as well as heat and salt in the summer season.

3.4 Experiment 2

3.4.1 Effect of tide (Case.1, 2)

Case.1 is a control case, which was executed under the boundary conditions explained in Section 2. For Case.2, we used the same boundary conditions but without consideration of the tide effect. The viscosity and diffusivity by tidal motion was not included and a quadratic bottom friction with the bottom drag coefficient of 0.0025 was used in Case.2.

Volume transports of the Kuroshio intrusion for Case.1 and Case.2 are shown in Fig. 11. Considering the effect of the M2 tide, the intrusion from the Kuroshio across the 200 m isobath line was considerably decreased. As shown in Figs. 11(b) and (c), the decrease of the Kuroshio intrusion mainly occurred east of Taiwan ($122\sim 123^\circ\text{E}$). Figure 12 shows the difference of velocity in the bottom layer between Case.1 and Case.2. The velocity near the bottom mainly decreased on the shelf region, and the decreased velocity amounts to ~ 10 cm/s northeast of Taiwan. The strong M2 tidal current east of Taiwan (Fig. 13) intensified the vertical viscosity, vertical diffusivity, and the bottom friction.

On the other hand, at the central part of the shelf break, $123\sim 127^\circ\text{E}$, the intrusion increased slightly in Case.1. This is due to the velocity of the M2 tidal current near the shelf break at $123\sim 127^\circ\text{E}$, which is smaller than

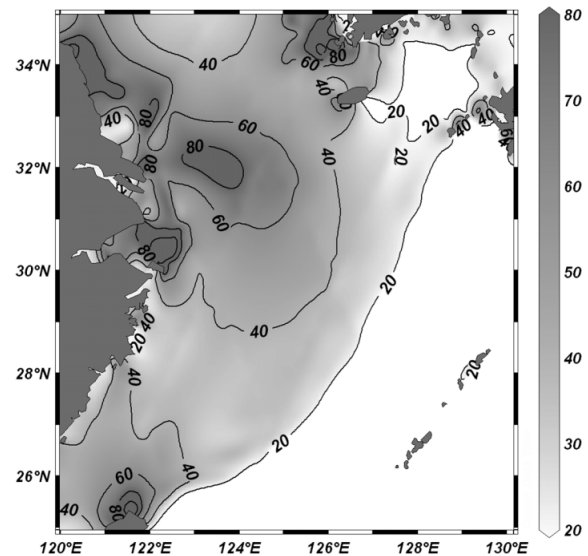


Fig. 13. Amplitude of the M2 tidal current calculated by the NAO.99Jb model (Matsumoto *et al.*, 2000).

the background current using the quadratic bottom friction in Case.2.

As for the intrusion into the shelf region in Case.2, the volume transport of the intrusion into the shelf area was calculated for four seasons: 0 Sv for winter, 0.24 Sv for spring, 0.21 Sv for summer, and 0.09 Sv for autumn. Although slightly larger than Case.1, these values are not very different from the transports estimated in Case.1. This suggests that tidal effects on the bottom friction could not exert a significant influence to depress the intrusion of the Kuroshio water into the shelf area.

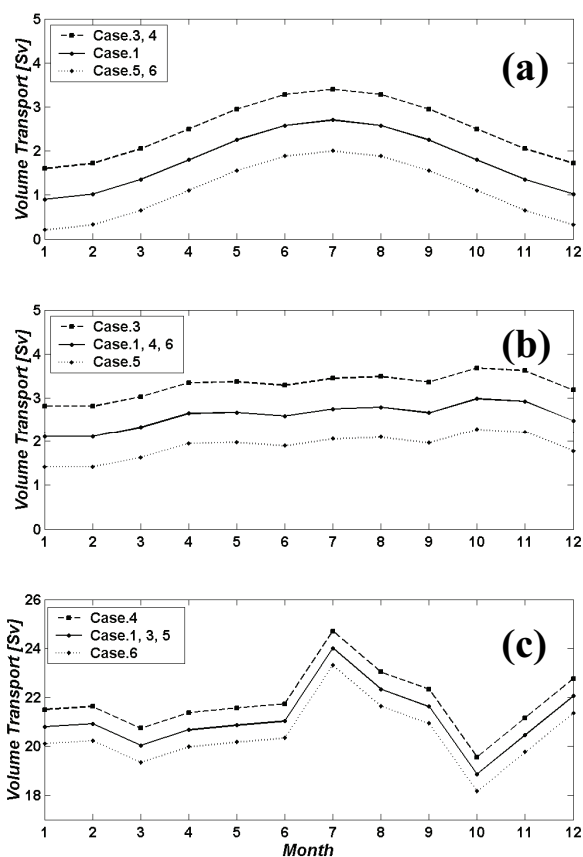


Fig. 14. Monthly value of each volume transport through (a) the Taiwan Strait, (b) the T/K Strait, and (c) the Tokara Strait for Case.1, 3, 4, 5, 6.

3.4.2 Effect of transport from the Taiwan Strait (Case.3, 4, 5, 6)

Volume transport from the Taiwan Strait has been disputed by many researchers. We adopted the result of Wang *et al.* (2003) with the maximum transport (2.7 Sv) in July and the minimum (0.9 Sv) in January. To investigate the effect of transport from the Taiwan Strait, four cases (Case.3, 4, 5, 6) were compared. Based on the boundary conditions of the control case (Case.1), Case.3, 4 increased the volume transport from the Taiwan Strait by as much as 0.7 Sv, while Case.5, 6 decreased it by 0.7 Sv through the whole year. We maintained the variation components of each transport and increased (or decreased) the average transport. The inflow transport from the east of Taiwan had the same value for all cases.

Case.3 (Case.5) set the increased (decreased) transport to flow out through the T/K Strait, and Case.4 (Case.6) set the increased (decreased) transport to flow out through the Tokara Strait, respectively. Figure 14 shows the transport through the Taiwan Strait, the T/K Strait, and the Tokara Strait for each case.

It is obvious that inflow through the Taiwan Strait causes outflow through the T/K Strait or the Tokara Strait. However, it is not yet clear how much the increased or decreased transport from the Taiwan Strait affects the T/K Strait or the Tokara Strait. We assumed four extreme cases in which the increased transport totally affects the T/K Strait (Case.3) or the Tokara Strait (Case.4), and the decreased transport totally affects the T/K Strait (Case.5) or the Tokara Strait (Case.6). The difference in transport from the Taiwan Strait between Case.3, 4 and Case.5, 6 is 1.4 Sv, however, as shown in Fig. 15(a), the difference of the intrusion from the Kuroshio region is smaller than

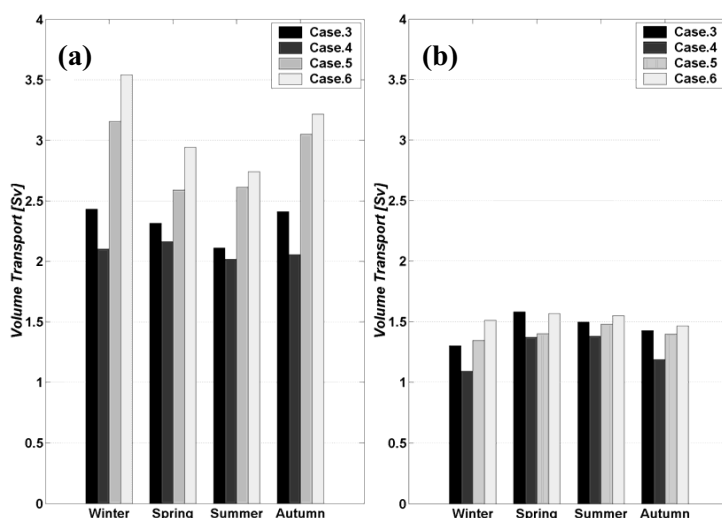


Fig. 15. Seasonal variation of the total intruded volume transport through the whole depth of the 200 m line (a), and through 80~200 m (b) for Case.3, 4, 5, 6.

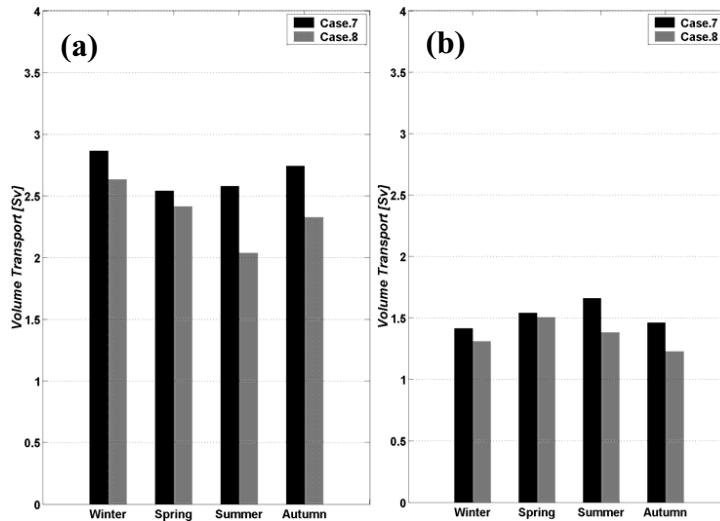


Fig. 16. Seasonal variation of the total intruded volume transport through the whole depth of the 200 m line (a), and through 80~200 m (b) for Case.7, 8.

that, especially in summer. This result shows that the intrusion from the Kuroshio is not totally controlled by the net transport between the Taiwan Strait and T/K Strait, leading us to conclude that the evaluation of the intruded transport from the Kuroshio is important to understand the nutrient supply from the Kuroshio into the ECS.

In spite of the large transport difference from the Taiwan Strait, the intrusion below 80 m did not change greatly, except during winter. This demonstrates that the transport from the Taiwan Strait mainly affects the intrusion only from the upper layer of the Kuroshio region, except during winter.

3.4.3 Effect of transport from east of Taiwan (Case.7, 8)

Lee *et al.* (2001) suggested that the seasonal cycle of the Kuroshio transport east of Taiwan is controlled by a combination of local along-channel wind forcing and Sverdrup forcing over the Philippine Sea. As a control case (Case.1), we adopted the result of Lee *et al.* (2001), which has seasonal variations of transport of 24 Sv in summer and a minimum transport of 20 Sv in autumn. And, two cases (Case.7, 8) were compared in order to clarify the effect of the transport variation of the Kuroshio. On the basis of the volume transport for Case.1, Case.7 (Case.8) increased (decreased) the volume transport from east of Taiwan by as much as 1.6 Sv. The inflow transports from the Taiwan Strait for Case.7 and Case.8 were the same as Case.1, and the outflow volume transport through the Tokara Strait increased (decreased) by as much as the increased (decreased) volume transport from east of Taiwan.

Figure 16 shows the volume transport of the Kuroshio intrusion through 0~200 m and 80~200 m for each case. When the transport from east of Taiwan was increased,

the intrusion from the Kuroshio also increased. With the inflow difference of 3.2 Sv from east of Taiwan for Case.7 and Case.8, the Kuroshio intrusion changed ~10% of the inflow difference (~0.4 Sv on an average).

4. Summary and Discussion

Intrusion from the Kuroshio onto the continental shelf of the ECS was investigated using a 3-D numerical model. The main objectives of this paper were to understand the behavior of the intruded Kuroshio water, to estimate the volume transport of the intrusion with seasonal variations, and to discuss the effect of tide and of transport from the Taiwan Strait and east of Taiwan.

As a method for evaluating the intrusion, passive tracer experiments were carried out. In the Preliminary Experiment a tracer was released in the Taiwan Strait, and from the vertical profile of the tracer, two vertical sections along the 200 m isobath line were determined for the release of tracers: 0~80 m and 80~200 m. In Exp. 1 and Exp. 2, the tracers were released at local sections along the 200 m isobath line for 30 days. The vertically integrated mass of the tracer was used to compare the horizontal distributions of the tracer for the control case. In addition, the intruded volume transports for each case were calculated using the time derivative of the total amount of water, including the passive tracer.

The tracer experiments for Case.1 (a control case) were discussed in Exp. 1 and clearly showed two main regions of the Kuroshio intrusion: northeast of Taiwan and west of Kyushu. From additional experiments for Case.1, which released the tracer for 90 days at the 200 m isobath line of 122~123°E, 123~124°E, and 124~125°E, it is realized that the tracer, intruded from 122°E to 123°E

through 80~200 m, shows the greatest seasonal difference of the horizontal distribution. In winter, the tracer intrudes solely south of 28°N, although it intrudes farther northward and flows into the small valley on the western ECS in summer. The spatial distribution with the 10-day interval of the tracer intruded from 122°E to 123°E shows that the intrusion flows downstream along the shelf edge or joins the Kuroshio in winter. On the other hand, the intrusion is divided into two paths in summer: northward flow along the small valley on the western ECS and a northeastward flow along the shelf edge. Intrusion also takes place at the central part of the continental shelf edge (123~127°E), but it does not affect the central ECS, and flows along the shelf break or is confined only to the shelf edge.

The total intruded volume transport through the 200 m isobath line was evaluated as 2.74 Sv in winter, 2.43 Sv in spring, 2.47 Sv in summer, and 2.84 Sv in autumn. The detailed tracer experiments show that the Kuroshio water affecting the shelf area shallower than 80 m mainly originates east of Taiwan (122~123°E), especially through the lower layer below 80 m. The intrusion into the shelf region is pushed actively in spring and in summer, although it does not reach the shelf area in the winter and flows down along the shelf break. In the summer, a part of the intruded Kuroshio water with a volume transport of 0.19 Sv flows into the shelf area. The transport is approximately three times greater than the volume transport of 0.06 Sv in summer from the Changjiang River. This suggests that the intruded Kuroshio water can be a nutrient source in the shelf area in summer.

The Kuroshio intrusion across the 200 m isobath line takes place all year round, but the intrusion into the shelf area shallower than 80 m only starts in spring and ends in autumn. What is the mechanism of summer season intrusion into the shelf area? The answer to this question could be obtained from the effect of stratification. In spite of the larger intrusion volume transport across the 200 m isobath line in winter, the intruded Kuroshio water across the 200 m isobath line was not transported into the shelf area shallower than 80 m. On the other hand, it intruded into the shelf area through the lower layer in summer, even though the intruded total volume transport across the 200 m isobath line was decreased in comparison with that in winter. Unlike high vertical viscosity in winter, the effect of stratification makes the vertical viscosity weak below the thermocline in summer. This effect could allow the Kuroshio water to intrude into the shelf area. The intruded water would be upwelled by the several mechanisms such as bottom friction layer, bottom topography, encroachment of the Taiwan Warm Current, and density gradient by the Changjiang discharge (Hu, 1994; Zhu, 2003; Lü *et al.*, 2006) near the Chinese coast, or by horizontal divergence of the Changjiang Dilute Water

(CDW) on the central ECS (Matsuno *et al.*, 2006). Thus, as suggested by Matsuno *et al.* (2006), it is expected that, due to the vertical process, the intruded Kuroshio water could contribute to increase the salinity of the CDW and also provide the nutrients into the euphotic zone resulting in biological production in the shelf region of the ECS.

The comparative studies in Exp. 2 allowed several components that affect the intrusion from the Kuroshio to be investigated. The tide effect is considered to intensify the linear bottom friction by Hunter's (1975) formula and the vertical eddy diffusivity and viscosity by James' (1977, 1978) method using M2 tidal velocity. The tide effect decreases the current velocity northeast of Taiwan and over the shelf, and the intrusion from the Kuroshio region is decreased in comparison to a case disregarding the tide effect. However, transportation of the intruded Kuroshio water into the central area of the shelf region is not significantly influenced by the tide induced bottom friction. The transport from the Taiwan Strait has a significant effect on the intrusion of the Kuroshio. However, the transport mainly affects the upper layer (0~80 m), while the effect on the lower layer is relatively small. The transport of the Kuroshio also has an important role as the Kuroshio water intrudes into the ECS. In this study the Kuroshio intrusion varied by ~10% inflow difference between two cases: an increased Kuroshio transport and a decreased transport. We set the volume transport of the Kuroshio to increase or decrease with the same vertical gradient calculated from the density structure itself to discount the effect of the vertical structure variation when the Kuroshio transport is changed. The contribution of the variation of vertical density gradient will be studied in a future experiment.

In this study we have confirmed the intrusion pattern from the Kuroshio by passive tracer experiments using a numerical model. The model only considered the local tide effect by simple parameterization which excludes the effect of the tidal residual current. In order to implement several cases, the model resolution was kept relatively low compared with previous studies, such as those of Guo *et al.* (2003, 2006) and Isobe and Beardsley (2006). However, this model has the advantage of simulating realistic motion on steep topography and the results have similar patterns to previous model studies and observations. More observations at the lower layer of the shelf region of ECS are needed in order to verify the model results.

Acknowledgements

We would like to thank Drs. J.-H. Yoon and N. Hirose of the Research Institute for Applied Mechanics (RIAM), Kyushu University, for providing us with the 3-D ocean model, RIAMOM. Thanks are also due to Drs. T. Senjyu, A. Isobe (Kyushu University, Japan) and H. J. Lee

(Korea Maritime University, Korea) for their valuable comments on this study. Finally, we would like to thank two anonymous reviewers.

References

- Barnier, B., L. Siefridt and P. Marchesiello (1995): Thermal forcing for a global ocean circulation model using a three-year climatology of ECMWF analyses. *J. Mar. Sys.*, **6**, 363–380.
- Boyer, T. P., C. Stephens, J. I. Antonov, M. E. Conkright, R. A. Locarnini, T. D. O'Brien and H. E. Garcia (2002): World Ocean Atlas 2001, Vol. 2, Salinity. *Tech. Rep., Atlas NESDIS*, **50**, Natl. Oceanic and Atmos. Admin., Washington, D.C., 165 pp.
- Chen, A. C.-T. and S.-L. Wang (1999): Carbon, alkalinity and nutrient budgets on the East China Sea continental shelf. *J. Geophys. Res.*, **104**(C9), 20675–20686.
- Chen, C., R. C. Beardsley, R. Limeburner and K. Kim (1994): Comparison of winter and summer hydrographic observations in the Yellow and East China Seas and adjacent Kuroshio during 1986. *Cont. Shelf Res.*, **14**, 909–929.
- Chern, C. S. and J. Wang (1992): The influence of Taiwan Strait waters on the circulation of the southern East China Sea. *La mer*, **30**, 223–228.
- Fang, G., B. Zhao and Y. Zhu (1991): Water volume transport through the Taiwan Strait and the continental shelf of the East China Sea measured with current meters. p. 345–358. In *Oceanography of Asian Marginal Seas*, ed. by K. Takano, Elsevier, Amsterdam.
- Grist, J. P. and S. A. Josey (2003): Inverse analysis adjustment of the SOC air-sea flux climatology using ocean heat transport constraints. *J. Climate*, **16**(20), 3274–3295.
- Guo, X., H. Hukuda, Y. Miyazawa and T. Yamagata (2003): A triply nested ocean model for simulating the Kuroshio-Roles of horizontal resolution on JEBAR. *J. Phys. Oceanogr.*, **33**, 146–169.
- Guo, X., Y. Miyazawa and T. Yamagata (2006): The Kuroshio onshore intrusion along the shelf break of the East China Sea: the origin of the Tsushima Warm Current. *J. Phys. Oceanogr.*, **36**, 2205–2231.
- Hsueh, Y., H.-J. Lie and H. Ichikawa (1996): On the branching of the Kuroshio west of Kyushu. *J. Geophys. Res.*, **101**, 3851–3857.
- Hu, D.-X. (1994): Some striking features of circulation in Huanghai Sea and East China Sea. *Oceanol. China Seas*, **11**, 27–38.
- Hunter, J. R. (1975): A note on quadratic friction in the presence of tides. *Estuar. Coast. Mar. Sci.*, **3**, 473–475.
- Hur, H. B., G. A. Jacobs and W. J. Teague (1999): Monthly water mass analyses in the Yellow and East China Seas. *J. Oceanogr.*, **55**, 171–184.
- Ishizaki, H. and T. Motoi (1999): Reevaluation of the Takano-Oonishi scheme for momentum advection of bottom relief in ocean models. *J. Atmos. Ocean. Technol.*, **16**, 1994–2010.
- Isobe, A. and R. C. Beardsley (2006): An estimate of the cross-frontal transport at the shelf break of the East China Sea with the Finite Volume Coastal Ocean Model. *J. Geophys. Res.*, **111**, C03012, doi:10.1029/2005JC003290.
- Isobe, A., E. Fujiwara, P.-H. Chang, K. Sugimatsu, M. Shimizu, T. Matsuno and A. Manda (2004): Intrusion of less saline shelf water into the Kuroshio subsurface layer in the East China Sea. *J. Oceanogr.*, **60**, 853–863.
- James, I. D. (1977): A model of the annual cycle of temperature in the frontal region of the Celtic Sea. *Estuar. Coast. Mar. Sci.*, **5**, 339–353.
- James, I. D. (1978): A note on the circulation induced by a shallow-sea front. *Estuar. Coast. Mar. Sci.*, **7**, 197–202.
- Katoh, O., K. Teshima, K. Kubota and K. Tsukiyama (1996a): Downstream transition of the Tsushima Current west of Kyushu in summer. *J. Oceanogr.*, **52**, 93–108.
- Katoh, O., K. Teshima, O. Abe, H. Fujita, K. Miyaji, K. Morinaga and N. Nakagawa (1996b): Process of the Tsushima Current formation revealed by ADCP measurements in summer. *J. Oceanogr.*, **52**, 491–507.
- Katoh, O., K. Morinaga and N. Nakagawa (2000): Current distributions in the southern East China Sea in summer. *J. Geophys. Res.*, **105**(C4), 8565–8573.
- Large, W. G. and S. Pond (1981): Open ocean momentum flux measurement in moderate to strong winds. *J. Phys. Oceanogr.*, **11**, 324–336.
- Lee, H. J., K. T. Jung, M. G. G. Foreman and J. Y. Chung (2000): A three-dimensional mixed finite-difference Galerkin function model for the oceanic circulation in the Yellow and the East China Sea. *Cont. Shelf Res.*, **20**, 863–895.
- Lee, H.-C., A. Rosati and M. J. Spelman (2006): Barotropic tidal mixing effects in a coupled climate model: Oceanic conditions in the Northern Atlantic. *Ocean Modell.*, **11**, 464–477.
- Lee, T. N., W. E. Johns, C.-T. Liu, D. Zhang, R. Zantopp and Y. Yang (2001): Mean transport and seasonal cycle of the Kuroshio east of Taiwan with comparison to the Florida Current. *J. Geophys. Res.*, **106**(C10), 22143–22158.
- Lie, H.-J. and C.-H. Cho (1994): On the origin of the Tsushima Warm Current. *J. Geophys. Res.*, **99**, 25081–25091.
- Lie, H.-J., C.-H. Cho, J.-H. Lee, P. Niller and J.-H. Hu (1998): Separation of the Kuroshio water and its penetration onto the continental shelf west of Kyushu. *J. Geophys. Res.*, **103**(C2), 2963–2976.
- Liu, K.-K., G.-C. Gong, C.-Z. Shyu, S.-C. Pai, C.-L. Wei and S.-Y. Chao (1992): Response of Kuroshio upwelling to the onset of the northeast monsoon in the sea north of Taiwan: Observations and a numerical simulation. *J. Geophys. Res.*, **97**(C8), 12511–12526.
- Lü, X., F. Qiao, C. Xia, J. Zhu and Y. Yuan (2006): Upwelling off Yangtze River estuary in summer. *J. Geophys. Res.*, **111**, C11S08, doi:10.1029/2005JC003250.
- Matsumoto, K., T. Takanezawa and M. Ooe (2000): Ocean tide models developed by assimilating TOPEX/POSEIDON altimeter data into hydrodynamical model: a global model and a regional model around Japan. *J. Oceanogr.*, **56**, 567–581.
- Matsuno, T., J.-S. Lee, M. Shimizu, S.-H. Kim and I.-C. Pang (2006): Measurements of the turbulent energy dissipation rate ϵ and an evaluation of the dispersion process of the Changjiang Diluted Water in the East China Sea. *J. Geophys. Res.*, **111**, C11S09, doi:10.1029/2005JC003196.
- Munk, W. H. and E. R. Anderson (1948): Notes on a theory of the thermocline. *J. Mar. Res.*, **7**(3), 276–295.
- Na, J. Y. and J. W. Seo (1998): The sea surface winds and heat

- fluxes in the East Asian marginal seas (a booklet for the data contained in the CD-ROM, 53 pp.).
- Noh, Y., C. J. Jang, T. Yamakata, P. C. Chu and C.-H. Kim (2002): Simulation of more realistic upper-ocean processes from an OGCM with a new ocean mixed layer model. *J. Phys. Oceanogr.*, **32**, 1284–1307.
- Oka, E. and M. Kawabe (1998): Characteristics of variations of water properties and density structure around the Kuroshio in the East China Sea. *J. Oceanogr.*, **54**, 605–617.
- Seung, Y. H. (1999): A geostrophic adjustment model of shelfward intrusion of oceanic upper water across a depth discontinuity: implication to the Kuroshio region. *Cont. Shelf Res.*, **19**, 247–269.
- Stephens, C., J. I. Antonov, T. P. Boyer, M. E. Conkright, R. A. Locarnini, T. D. O'Brien and H. E. Garcia (2002): World Ocean Atlas 2001, Vol. 1, Temperature. *Tech. Rep., Atlas NESDIS*, **49**, Natl. Ocean and Atmos. Admin., Washington, D.C., 167 pp.
- Takikawa, T. and J.-H. Yoon (2005): Volume transport through the Tsushima Straits estimated from sea level difference. *J. Oceanogr.*, **61**, 699–708.
- Tang, T. Y., Y. Hsueh, Y. J. Yang and J. C. Ma (1999): Continental slope flow northeast of Taiwan. *J. Phys. Oceanogr.*, **29**, 1353–1362.
- Tang, T. Y., J. H. Tai and Y. J. Yang (2000): The flow pattern north of Taiwan and the migration of the Kuroshio. *Cont. Shelf Res.*, **20**, 349–371.
- Wang, Y. H., S. Jan and D. P. Wang (2003): Transports and tidal current estimates in the Taiwan Strait from the shipboard ADCP observations (1999–2001). *Estuar. Coast. Shelf Sci.*, **57**, 193–199.
- Webb, D. J., B. A. de Cuevas and C. S. Richmond (1998): Improved advection schemes for ocean models. *J. Atmos. Ocean. Technol.*, **15**, 1171–1187.
- Yanagi, T., T. Shimizu and H.-J. Lie (1998): Detailed structure of the Kuroshio frontal eddy along the shelf edge of the East China Sea. *Cont. Shelf Res.*, **18**, 1039–1056.
- Zhu, J. (2003): Dynamic mechanism of the upwelling on the west side of the submerged river valley off the Yangtze mouth in summertime. *Chin. Sci. Bull.*, **48**, 2754–2758.